



Sub-attosecond time delays of photoemission from asymmetric cores of molecules

Yidian Tian ^{1,2,3}, Yibo Hu,¹ Yueming Zhou,¹ Peixiang Lu,¹ and Kunlong Liu ^{2,3,*}¹*School of Physics and Wuhan National Laboratory for Optoelectronics, Huazhong University of Science and Technology, Wuhan 430074, China*²*School of Physical Sciences, Great Bay University, Dongguan 523000, China*³*Great Bay Institute for Advanced Study, Dongguan 523000, China*

(Received 30 June 2024; accepted 21 October 2024; published 18 November 2024)

We theoretically study the extreme ultraviolet (XUV) photoemission of the asymmetric molecular ion HeH^{2+} beyond the dipole approximation. Based on the double-slit interference of the photoelectron emitted from two atomic cores, we propose a scheme to obtain the XUV photoemission time delays originated from different physical mechanisms. In our study, two types of sub-attosecond photoemission time delays are identified and extracted from the observable photoelectron momentum distributions. One is the so-called birth time delay, originated from the travel time of the photon across the molecule, and the other is the escaping time delay of the photoelectron from two different cores. The present study shows the observable evidence demonstrating that in single-photon ionization, it takes more time for the photoelectron escaping from the helium nucleus than that from the proton.

DOI: [10.1103/PhysRevResearch.6.043150](https://doi.org/10.1103/PhysRevResearch.6.043150)

I. INTRODUCTION

Time-resolved measurement performed on quantum systems is one of the most fascinating topics in the attophysics community. Since the attosecond pulses of extreme ultraviolet (XUV) radiation is experimentally accessible via the high-order harmonic generation process [1–5], scientists are now able to uncover the microscopic dynamical processes on the attosecond ($1 \text{ as} = 10^{-18} \text{ s}$) and even zeptosecond ($1 \text{ zs} = 10^{-21} \text{ s}$) timescales [6–9]. In quantum mechanics, the physical quantity of time enters the expression of the wave function as a phase term, indicating that the photoemission time delay is directly linked to the phase shift of the electronic wave function in the ionization process [10]. Therefore, extracting the phase shifts for photoelectrons is the key to studying the time delays in XUV photoemission.

Yet, the phase of the electronic wave function is not directly measurable in experiments. In previous studies, the techniques of attosecond streaking [11–14] and reconstruction of attosecond beating by interference of two-photon transitions (RABITT) [15–19] are two prevailing approaches to study the photoemission time delays. In both methods, a weak near-infrared streaking pulse with adjustable time delay is required for the extraction of the XUV ionization delay. However, it is pointed out [20–24] that the participation of the near-infrared pulse introduces the additional Coulomb-laser coupling

phase, which needs to be ruled out to obtain the photoemission delay. In the present work, alternatively, we demonstrate that it is possible to extract the phase shift and the ionization time delays between the electronic wave packets from two different atomic cores via the double-slit interferometric method, without additionally applying the streaking fields.

When a diatomic molecule interacts with the XUV pulse, as shown in Fig. 1, the electronic wave packets are emitted from two cores, eventually forming a double-slit interference pattern in the photoelectron momentum distribution (PMD) [25–31]. In principle, the information regarding the internuclear distance and the phase shift between two wave packets is imprinted in the interference pattern. In the special case of symmetric molecules, the phase shift is associated with the birth time delay caused by the nondipole effect [9]. It is shown that the birth time delay can be obtained from its relation to the interference maxima or minima of the PMDs and the internuclear distance [9,32,33]. In more general cases of asymmetric molecules, however, the weights of two coherent wave packets differ from each other. As a result, the phase shift between two electronic wave packets is no longer simply related to the interference maxima or minima of the PMDs. Moreover, the time delay for the photoelectron escaping from two different cores would additionally introduce the phase shift between the ionizing wave packets, as indicated by the solid and dashed oscillating curves in Fig. 1. Therefore, to study the XUV photoemission delays of asymmetric diatomic molecules, one needs not only to extract the total phase shift from the interference pattern, but also to identify the respective contributions of the time delays of different mechanisms. To this end, a scheme is proposed to obtain the phase shifts of the wave packets emitted from two different cores, based on the Fourier analysis of the double-slit interference patterns of the observable PMDs. By further taking advantage of the underlying physical

*Contact author: liukunlong@gbu.edu.cn

Published by the American Physical Society under the terms of the [Creative Commons Attribution 4.0 International license](https://creativecommons.org/licenses/by/4.0/). Further distribution of this work must maintain attribution to the author(s) and the published article's title, journal citation, and DOI.

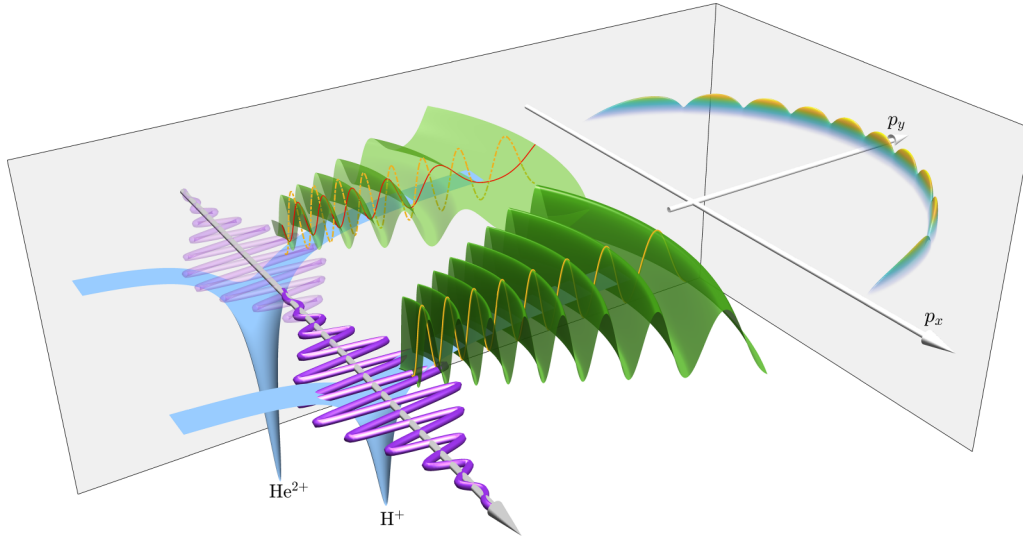


FIG. 1. The physical picture of the photoemission of HeH^{2+} driven by an XUV pulse. When the pulse propagates along the molecular axis and interacts with the molecule, the coherent electronic wave packets are emitted from two cores with a phase shift, due to the so-called birth time delay [9] as the photon travels across the molecule with the speed of light. Then, the outgoing wave packets propagate on different Coulomb potentials of two cores of the molecule, leading to an additional phase shift between them, as indicated by the solid and dashed oscillating curves. Eventually, the information of the total phase shift and the internuclear distance is imprinted in the modulated photoelectron momentum distribution of single-photon ionization. Based on the double-slit interference model, it is possible to extract the encoded information from the interference pattern. See the main text for details.

mechanisms, we demonstrate that two types of sub-attosecond time delays in the XUV photoemission of the asymmetric molecular ion HeH^{2+} can be identified and extracted.

II. NUMERICAL METHOD

We numerically solve the nondipole two-dimensional (2D) time-dependent Schrödinger equation (TDSE) in the Cartesian coordinate system for HeH^{2+} aligned along the x axis. For the nondipole TDSE, the incident pulse propagating in time and space is accounted and, in the present study, the XUV laser pulse is linearly polarized in the y direction and propagates towards the $+x$ direction. The nondipole TDSE is given by (in atomic units) [34]

$$i \frac{\partial}{\partial t} \Psi(\mathbf{r}, t) = \left\{ \frac{1}{2} [-i\nabla + \mathbf{A}(\eta)]^2 + V_0(\mathbf{r}) \right\} \Psi(\mathbf{r}, t), \quad (1)$$

where $\Psi(\mathbf{r}, t)$, $\mathbf{r} = (x, y)$, $\mathbf{A}(\eta)$, and $V_0(\mathbf{r})$ represent the electronic wave function, the coordinate of the electron, the vector potential of the laser pulse, and the Coulomb potential, respectively. To reproduce the ionization potential of HeH^{2+} in its first excited state at different internuclear distance, the modified soft-core potential in the following is used [35]:

$$V_0(\mathbf{r}) = \frac{-Z_L}{1/a(R) - a(R)/b + \sqrt{x_+^2 + y^2 + [a(R)/b]^2}} + \frac{-Z_R}{1/a(R) - a(R)/b + \sqrt{x_-^2 + y^2 + [a(R)/b]^2}}, \quad (2)$$

with $x_{\pm} = x \pm R/2$ and $Z_{L,R}$ being the locations and charger numbers of the left and right cores of the molecule, respectively. $a(R)$ and $b = 5$ are the soft-core parameters. In our calculations, $a(R)$ is adjusted at the different internuclear

distances to reproduce the ionization potentials of HeH^{2+} in its first excited state at the corresponding R [36]. The vector potential of the XUV laser pulse is given by

$$\mathbf{A}(\eta) = A_y(\eta) \mathbf{e}_y = \frac{\mathcal{E}}{\omega} \sin^4 \left(\frac{\pi \eta}{NT} \right) \cos(\eta) \mathbf{e}_y, \quad (3)$$

with $\eta = \omega(t - x/c)$ where c is the speed of light in vacuum, and ω , $T = 2\pi/\omega$, \mathcal{E} , and N indicate the laser frequency, the optical cycle, the electric field amplitude, and the number of the optical cycles of the full pulse, respectively. In the present simulations, the laser parameters are chosen as $\omega = 29.40$ a.u. (corresponding to the photon energy of 800 eV), $\mathcal{E} = 23.87$ a.u. (corresponding to the intensity of 2×10^{19} W/cm²), and $N = 50$ unless stated otherwise. Noted that the light propagating in time and space is included within the definition of the laser vector potential given in Eq. (3).

The nondipole TDSE is numerically solved using the split-operator spectral method with modifications [33,37], in order to deal with the space-dependent vector potential. The initial stationary wave functions are obtained by the imaginary-time propagation method. The real-time propagation includes two parts: the interaction and the free propagation afterwards. For the interaction part, the evolution starts when the XUV pulse enters the box of the 2D grid and ends when the tail of the pulse leaves the box. We have chosen a 2D grid large enough to contain the majority of the ionizing wave packets until the interaction process ends. This is guaranteed and has been verified in our calculations. After the interaction, we continue the evolution of the wave function without external fields and apply the absorbing potential to split the outgoing wave packets. In this case, one can solve the TDSE and obtain the photoelectron momentum distributions in the conventional way [38,39]. Regarding the simulation parameters, there are

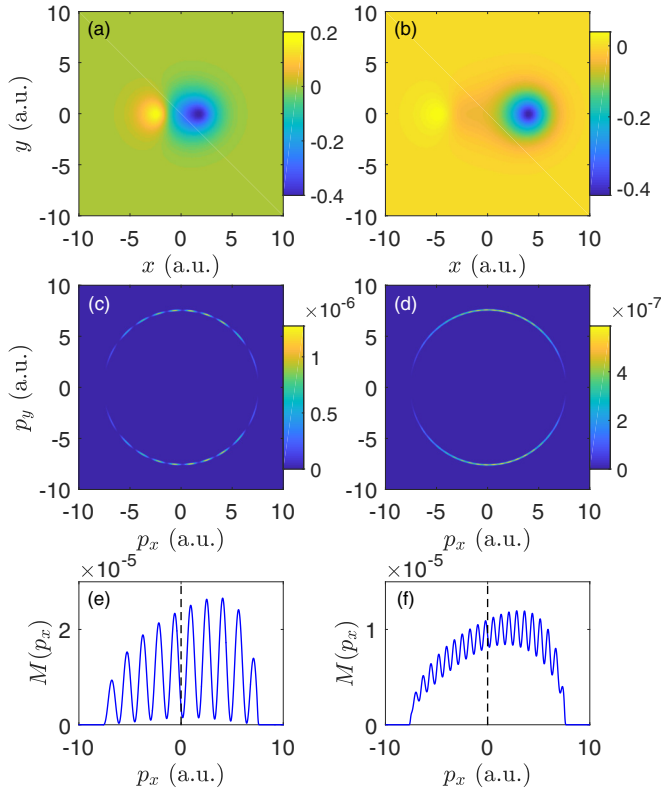


FIG. 2. (a) and (b) The initial wave functions of the first excited state of HeH^{2+} . (c) and (d) The photoelectron momentum distributions for the interactions of HeH^{2+} with the XUV laser pulse, which is polarized along the y axis and propagates towards the $+x$ direction. (e) and (f) The integrated momentum distributions as a function of p_x . The results shown in the left and right columns correspond to the internuclear distances of $R = 3.89$ a.u. and $R = 8$ a.u., respectively.

4000×4000 grid points of the box. The spacing steps are $\Delta x = \Delta y = 0.1$ a.u. The time step for the evolution of the wave function is chosen as $\delta t = 0.005$ a.u.

III. RESULTS AND DISCUSSION

By numerically solving the TDSE beyond the dipole approximation, we calculate the PMDs for the photoionization of the asymmetric molecular ion HeH^{2+} driven by XUV pulses. As we are focusing on the electronic dynamics on the sub-attosecond timescale, the nuclei would barely move within such short duration. Here, in each calculation, the internuclear distance is fixed at R . To compare intuitively the results for the equilibrium internuclear distance and those for a larger internuclear distance, we show in Figs. 2(a) and 2(b) the initial wave functions of HeH^{2+} in the $2p\sigma$ excited state at $R = 3.89$ a.u. (the equilibrium internuclear distance) and $R = 8$ a.u., respectively. Accordingly, the PMDs are shown in Figs. 2(c) and 2(d). The ring structures with modulations can be observed in the PMDs. Meanwhile, the modulation becomes denser as the internuclear distance is increased. It is a typical feature of the double-slit interference in single-photon ionization of diatomic molecules.

To extract the desired information from the interference patterns, we start with writing the wave functions of

the photoelectron emitted from the left and right nuclei, respectively, as [33,40–42]

$$\begin{aligned} \Psi_L(\mathbf{p}) &= A_L(\mathbf{p}) \\ &\times \exp\{i[\mathbf{p} \cdot \mathbf{r}_L - E_k(t - \tau_L) - E_k\tau_b + \phi_0]\}, \quad (4) \\ \Psi_R(\mathbf{p}) &= A_R(\mathbf{p}) \\ &\times \exp\{i[\mathbf{p} \cdot \mathbf{r}_R - E_k(t - \tau_R) - E_0\tau_b]\}. \quad (5) \end{aligned}$$

Here, $E_k = \mathbf{p}^2/2$, E_0 , and $\mathbf{r}_{L,R} = \mathbf{r} \pm \mathbf{R}_e/2$ indicate the final kinetic energy of the photoelectron, the binding energy of the initial state, and the emitting locations of the photoelectron, respectively. Note that \mathbf{R}_e instead of \mathbf{R} is used for the equations because the effective double-slit distance \mathbf{R}_e might differ from the internuclear distance \mathbf{R} [32]. τ_b indicates the birth time delay originated from the travel time of the photon across the molecule and $\tau_{L,R}$ the time delays of the half-collision [20] of the photoelectron in the Coulomb potentials of two cores. $\phi_0 = \pi$ is the initial phase shift due to the wave function of the first excited state of HeH^{2+} . Then, the photoelectron momentum distribution can be written as

$$\begin{aligned} M(\mathbf{p}) &= |\Psi_L(\mathbf{p}) + \Psi_R(\mathbf{p})|^2 \\ &= |A_L(\mathbf{p})|^2 + |A_R(\mathbf{p})|^2 \\ &\quad + A_m(\mathbf{p}) \exp[+i(p_x R_e + \phi_\tau + \phi_0)] \\ &\quad + A_m(\mathbf{p}) \exp[-i(p_x R_e + \phi_\tau + \phi_0)], \quad (6) \end{aligned}$$

with

$$\phi_\tau = -(E_k - E_0)\tau_b + E_k(\tau_L - \tau_R) \quad (7)$$

and $A_m(\mathbf{p}) = A_L(\mathbf{p})A_R(\mathbf{p})$. Note that in Eq. (6) we have applied $\mathbf{p} \cdot (\mathbf{r}_L - \mathbf{r}_R) = \mathbf{p} \cdot \mathbf{R}_e = p_x R_e$ since the molecule is aligned along the x axis.

On the right-hand side of Eq. (6), we can see that the sum of the third and fourth terms plays the role of modulating the PMDs in the dimension of p_x . This feature can be observed clearly in Figs. 2(e) and 2(f), where we show the momentum distributions $M(p_x)$ by integrating the 2D PMDs over the p_y direction. In contrast to the XUV ionization of H_2^+ [32,33], the minima of the distributions $M(p_x)$ for HeH^{2+} are nonzero, due to the different weights of two coherent wave packets. In this case, as mentioned previously, knowing the maxima or minima of the modulated PMDs is no longer sufficient to obtain the physical information encoded in the phase terms of Eq. (6).

In the following, we introduce the method that allows us to extract the values of R_e and ϕ_τ simultaneously from the observable $M(p_x)$. The extraction procedure includes three steps. First, by applying the Fourier transformation to $M(p_x)$, we have

$$\begin{aligned} \hat{G}(f_{p_x}) &= \mathcal{F}[M(p_x)] \\ &= \hat{G}_0(f_{p_x}) + \hat{G}_+(f_{p_x}) + \hat{G}_-(f_{p_x}) \\ &= \mathcal{F}[|A_L(p_x)|^2 + |A_R(p_x)|^2] \\ &\quad + \mathcal{F}\{A_m(p_x) \exp[+i(p_x R_e + \phi_\tau + \phi_0)]\} \\ &\quad + \mathcal{F}\{A_m(p_x) \exp[-i(p_x R_e + \phi_\tau + \phi_0)]\}. \quad (8) \end{aligned}$$

On the right-hand side of Eq. (8), $\hat{G}_0(f_{p_x})$ contributes to the Fourier spectrum centered at the $f_{p_x} = 0$ since the

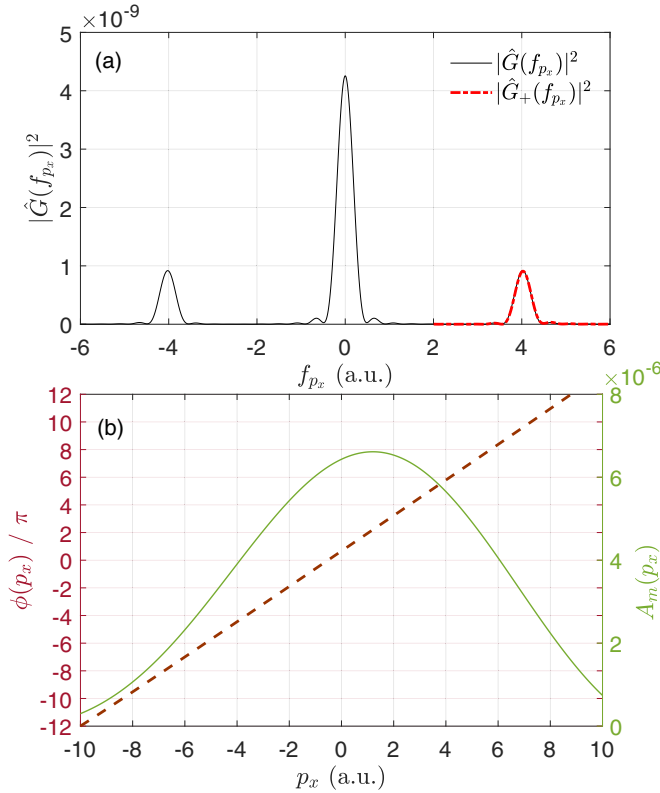


FIG. 3. (a) The spectrum of $\hat{G}(f_{p_x})$ obtained from the Fourier transformation of the momentum distribution $M(p_x)$ shown in Fig. 2(e), together with the spectrum of $\hat{G}_+(f_{p_x})$ filtered out from $\hat{G}(f_{p_x})$ by a step function. (b) The phase and the amplitude as a function of p_x extracted from the inverse Fourier transformation of $\hat{G}_+(f_{p_x})$. According to Eq. (8), R_e equals the slope of $\phi(p_x)$, and the value of $\phi(p_x = 0)$ equals $\phi_\tau + \phi_0$.

amplitudes $A_{L,R}(p_x)$ are typically Gaussian-like distributions for single-photon ionization, while $\hat{G}_\pm(f_{p_x})$ results in the Fourier spectra peaked at around $f_{p_x} = \pm R_e$ due to the oscillating terms $\pm p_x R_e$ of the phase. Second, as long as the distributions of $\hat{G}_0(f_{p_x})$ and $\hat{G}_\pm(f_{p_x})$ are well separated in the spectrum, one can filter out the data of $\hat{G}_\pm(f_{p_x})$ and apply the inverse Fourier transformation. Given that $\mathcal{F}^{-1}[\hat{G}_\pm(f_{p_x})] = A_m(p_x) \exp[\pm i(p_x R_e + \phi_\tau + \phi_0)]$, one can obtain the amplitude $A_m(p_x)$ and the phase $\phi(p_x) = R_e p_x + (\phi_\tau + \phi_0)$ in this step. Finally, as the phase $\phi(p_x)$ is a linear function of p_x , one can easily find from the data the slope R_e and the value of $\phi(p_x = 0) = \phi_\tau + \phi_0$.

As an example to demonstrate the Fourier analysis method discussed above, we analyze the PMD data [shown in Fig. 2(e)] for the XUV ionization of HeH^{2+} at its internuclear distance $R = 3.89$ a.u. We calculate the Fourier transformation of $M(p_x)$ and show the corresponding spectrum $|\hat{G}(f_{p_x})|^2$ in Fig. 3(a). It is clear that $|\hat{G}(f_{p_x})|^2$ consists of three well-separated peaks, corresponding to three different oscillation frequencies of $M(p_x)$, which are consistent with Eq. (6) and the discussion above. Note that in this step both the amplitude and the phase of $\hat{G}(f_{p_x})$ are obtained from the calculation. Next, we filter out $\hat{G}_+(f_{p_x})$ by applying a step function to $\hat{G}(f_{p_x})$, as indicated by the dash-dotted curve in Fig. 3(a).

Given that $\hat{G}_+(f_{p_x}) = \mathcal{F}\{A_m(p_x) \exp[+i(p_x R_e + \phi_\tau + \phi_0)]\}$ according to the Eq. (8), by performing the inverse Fourier transformation of $\hat{G}_+(f_{p_x})$, we can obtain the amplitude $A_m(p_x)$ and, more importantly, the phase $\phi(p_x)$. The results are shown in Fig. 3(b). It is clear that the extracted phase indeed shows the linear dependence on p_x . Finally, via linear regression analysis of the data of the extracted phase, the slope for R_e and the value of $\phi(p_x = 0) = \phi_\tau + \phi_0$ can be obtained.

Based on the analysis above, the phase shift ϕ_τ between the wave packets emitted from two nuclei of the molecule can be obtained from the double-slit interfered PMD. Yet, according to Eq. (7), two unknown variables need to be determined: the birth time delay τ_b and the escaping time delay $\tau_C = \tau_L - \tau_R$ from two atomic cores. The latter one is vanishing for symmetric molecules, in which case one can obtain τ_b straightforwardly from the extracted ϕ_τ , without relying on measuring the internuclear distance. Such advantage of the present scheme will enhance the reliability of extracting the time delays, since the effective double-slit distance R_e for the emitting wave packets differs from the molecular internuclear distance in some situations [32].

For the asymmetric molecule HeH^{2+} , however, τ_C is not vanishing. Thus, we need two sets of data to resolve τ_b and τ_C from the phase shift ϕ_τ . To this end, the molecule is orientated in the opposite directions along the x axis for two sets of simulations, respectively, while the XUV pulse always propagates towards the $+x$ direction. According to Eq. (7), the electronic phase shifts in these two scenarios are written, respectively, as

$$\phi_\tau^{\text{HeH}} = -(E_k - E_0)\tau_b + E_k\tau_C, \quad (9)$$

$$\phi_\tau^{\text{HHe}} = -(E_k - E_0)\tau_b - E_k\tau_C, \quad (10)$$

where $\tau_C \equiv \tau_{\text{He}} - \tau_{\text{H}}$ indicates the escaping time delay for the photoelectron from two cores. The superscripts (HeH and HHe) indicate two opposite orientations of the molecule along the x axis. Then, by solving the equation set of Eqs. (9) and (10), one can eventually obtain the time delays τ_b and τ_C , which are given by

$$\tau_b = \frac{\phi_\tau^{\text{HeH}} + \phi_\tau^{\text{HHe}}}{-2(E_k - E_0)}, \quad (11)$$

$$\tau_C = \frac{\phi_\tau^{\text{HeH}} - \phi_\tau^{\text{HHe}}}{2E_k}. \quad (12)$$

One can see that the time delays are eventually given by the phase shifts encoded in PMDs divided by energy. It can be understood in the following way. For the wave functions of free electrons, the phase term is accumulated via the energy times time in general. Then, the phase shift between two coherent electronic wave packets at constant energy will reflect the time delay between them. As a result, the time delays based on the phase shifts extracted from PMDs would have the form of a phase shift divided by energy. According to Eqs. (11) and (12), one can determine two types of time delays by measuring the PMDs for the oppositely orientated HeH^{2+} .

In Fig. 4(a), we show the extracted phase shift ϕ_τ as a function of the internuclear distance. The results are obtained from the corresponding PMDs for the XUV ionization of HeH^{2+} under two opposite orientations, based on the

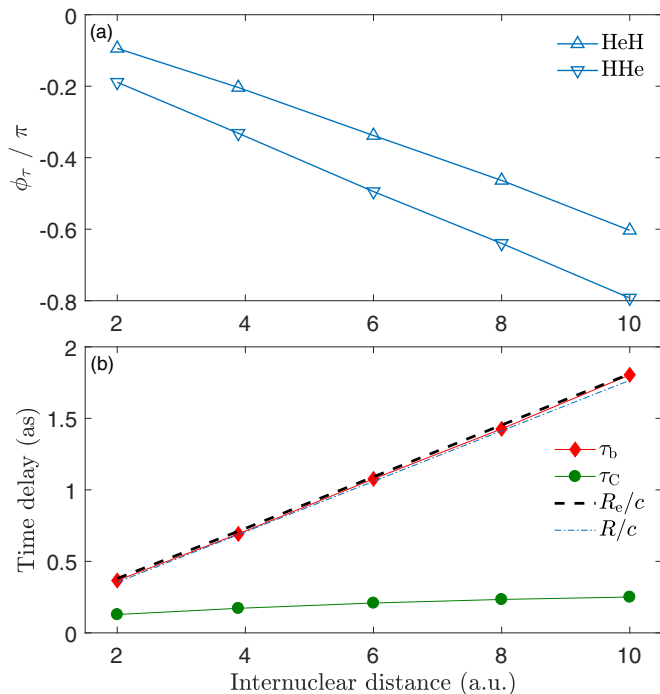


FIG. 4. (a) The phase shift ϕ_τ between the photoelectron wave packets emitted from two cores as a function of internuclear distance. The results for two opposite orientations of the molecule are shown. (b) The time delays for the photoemission of HeH^{2+} . See the main text for details.

extraction scheme discussed above. Accordingly, the time delays, τ_b and τ_C , are calculated based on Eqs. (11) and (12) with the extracted phase shifts. The results are showed in Fig. 4(b). For comparison, we show the delay given by R_e/c and R/c , where R_e is also extracted from the PMDs and R is the internuclear distance used in the simulation. One can see that the extracted birth time delays τ_b agree with R_e/c and R/c very well. The deviation between them is less than 2% in our simulations. It demonstrates the reliability of the present scheme of data extraction from the observable PMDs. On the other hand, our result shows that the nonvanishing photoemission time delay τ_C is positive and generally below one attosecond under the photon energy of 800 eV. It suggests that it takes more time for the photoelectron escaping from the He core than from the H core. This is reasonable since the Coulomb attraction of He^{2+} to the photoelectron is stronger than that of a proton. In addition, τ_C becomes smaller as the internuclear distance decreases. This is because at small internuclear distances the Coulomb potentials of two nuclei overlap with each other and the difference between the Coulomb potentials at two nuclear locations is not as much as those when two nuclei are well separated.

Based on the present scheme for extracting time delays from the PMDs, we further study the dependence of the photoemission delays of HeH^{2+} on the photon energy ranging from 600–1600 eV. The phase shifts ϕ_τ and the time delays for the cases of the equilibrium internuclear distance ($R = 3.89$ a.u.) and larger internuclear distance ($R = 10$ a.u.) are shown in the left and right columns of Fig. 5, respectively. For both cases, the extracted birth time delays agree generally with

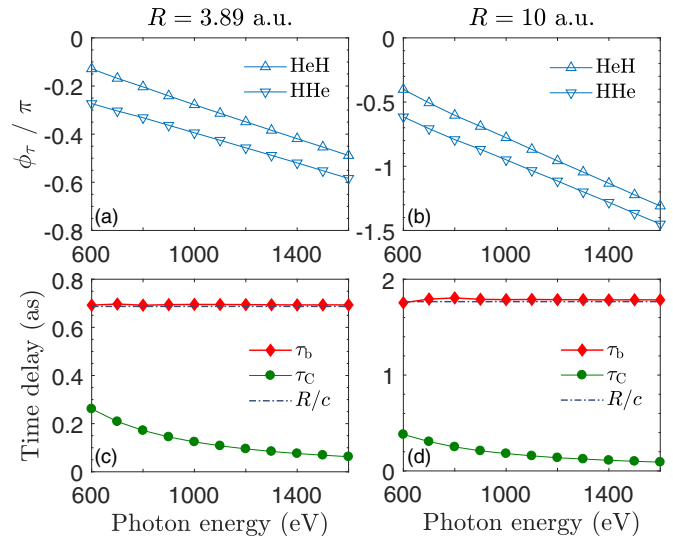


FIG. 5. The phase shift ϕ_τ and the photoemission time delays as a function of the photon energy of the XUV pulse. The results for the molecule at two internuclear distances are shown in the left and right columns, respectively.

the corresponding travel time R/c of the photon across the molecule, independent of the photon energy. On the other hand, we can see the increasing tendency for the escaping time delay τ_C as the photon energy reduces. It can be attributed to the higher impact of the Coulomb potentials on the slower photoelectrons. The observed tendency indicates that it takes more additional time for the slower photoelectron to escape from the He core with respect to that from the H core.

So far, we have showed two types of photoemission time delays originating from different mechanisms for asymmetric diatomic molecular systems. First, the birth time delay of photoelectrons is due to the travel time of the photon across two nuclei of the molecule. As the speed of light is constant, the extracted birth time delay is insensitive to the laser parameters. Instead, the birth time delay depends on the molecular internuclear distance. Second, the time delay for photoelectrons escaping from two cores depends on the Coulomb attraction of the cores as well as the kinetic energy of the photoelectron. Thus, the escaping time delay would be sensitive to the details of the Coulomb potential and the photon energy of the driving pulse.

IV. CONCLUSION

In conclusion, we have studied the photoionization of the asymmetric molecular ion HeH^{2+} driven by XUV laser pulses and focus on the time delays for the photoelectrons emitted from different atomic cores. By analyzing the photoelectron momentum distributions, we propose and demonstrate a scheme to extract the phase shift of the ionizing wave packets, based on the double-slit interference. It is further shown that the birth time delay and the escaping time delay for the photoelectron emitted from two cores can be distinguished and obtained. As only one XUV laser pulse is

used in the present study, our scheme excludes the effect of streaking fields that is unavoidable in the attosecond streaking or RABITT. Our study presents the direct evidence from observables and demonstrates that it takes more time for the photoelectron escaping from the He^{2+} than that from the proton.

The proposed scheme for extracting time delays is primarily associated with the double-slit interference of photoelectrons and does not rely on the chosen molecular system or theoretical models. Therefore, although the simulation in the present study is based on a two-dimensional model of HeH^{2+} , our scheme would be generalized to other diatomic molecular systems in three-dimensional cases, as long as the double-slit interference patterns of photoelectrons are observable. The proposed scheme in the present work provides the access to resolving the sub-attosecond dynamics

for future experimental studies on ultrafast strong-field phenomena.

The data that support the plots within this paper and other findings of this study are available from the contact author upon reasonable request.

ACKNOWLEDGMENTS

This work is supported by National Natural Science Foundation of China (Grants No. 12174133, No. 11874163, No. 12021004) and the Innovation Project of Optics Valley Laboratory (Grant No. OVL2021ZD001). The computing work in this paper is supported by the public computing service platform provided by Network and Computing Center of HUST.

Y.T. and Y.H. contributed equally to this work.

-
- [1] M. Ferray, A. L'Huillier, X. F. Li, L. A. Lompré, G. Mainfray, and C. Manus, Multiple-harmonic conversion of 1064 nm radiation in rare gases, *J. Phys. B: At. Mol. Opt. Phys.* **21**, L31 (1988).
- [2] P. M. Paul, E. S. Toma, P. Breger, G. Mullot, F. Augé, Ph. Balcou, H. G. Muller, and P. Agostini, Observation of a train of attosecond pulses from high harmonic generation, *Science* **292**, 1689 (2001).
- [3] F. Krausz and M. Ivanov, Attosecond physics, *Rev. Mod. Phys.* **81**, 163 (2009).
- [4] G. Sansone, E. Benedetti, F. Calegari, C. Vozzi, L. Avaldi, R. Flammini, L. Poletto, P. Villoresi, C. Altucci, R. Velotta, S. Stagira, S. De Silvestri, and M. Nisoli, Isolated single-cycle attosecond pulses, *Science* **314**, 443 (2006).
- [5] E. Goulielmakis, M. Schultze, M. Hofstetter, V. S. Yakovlev, J. Gagnon, M. Uiberacker, A. L. Aquila, E. M. Gullikson, D. T. Attwood, R. Kienberger, F. Krausz, and U. Kleineberg, Single-cycle nonlinear optics, *Science* **320**, 1614 (2008).
- [6] M. Schultze, M. Fieß, N. Karpowicz, J. Gagnon, M. Korbman, M. Hofstetter, S. Neppl, A. L. Cavalieri, Y. Komninos, Th. Mercouris, C. A. Nicolaides, R. Pazourek, S. Nagele, J. Feist, J. Burgdörfer, A. M. Azzeer, R. Ernstorfer, R. Kienberger, U. Kleineberg, E. Goulielmakis, F. Krausz *et al.*, Delay in photoemission, *Science* **328**, 1658 (2010).
- [7] K. Klünder, J. M. Dahlström, M. Gisselbrecht, T. Fordell, M. Swoboda, D. Guénot, P. Johnsson, J. Caillat, J. Mauritsson, A. Maquet, R. Taïeb, and A. L'Huillier, Probing single-photon ionization on the attosecond time scale, *Phys. Rev. Lett.* **106**, 143002 (2011).
- [8] P. Eckle, A. N. Pfeiffer, C. Cirelli, A. Staudte, R. Dörner, H. G. Muller, M. Büttiker, and U. Keller, Attosecond ionization and tunneling delay time measurements in Helium, *Science* **322**, 1525 (2008).
- [9] S. Grundmann, D. Trabert, K. Fehre, N. Strenger, A. Pier, L. Kaiser, M. Kircher, M. Weller, S. Eckart, L. P. H. Schmidt, F. Trinter, T. Jahnke, M. S. Schöffler, and R. Dörner, Zeptosecond birth time delay in molecular photoionization, *Science* **370**, 339 (2020).
- [10] E. P. Wigner, Lower limit for the energy derivative of the scattering phase shift, *Phys. Rev.* **98**, 145 (1955).
- [11] M. Drescher, M. Hentschel, R. Kienberger, G. Tempea, C. Spielmann, G. A. Reider, P. B. Corkum, and F. Krausz, X-ray pulses approaching the attosecond frontier, *Science* **291**, 1923 (2001).
- [12] R. Kienberger, E. Goulielmakis, M. Uiberacker, A. Baltuska, V. Yakovlev, F. Bammer, A. Scrinzi, T. Westerwalbesloh, U. Kleineberg, U. Heinzmann, M. Drescher, and F. Krausz, Atomic transient recorder, *Nature (London)* **427**, 817 (2004).
- [13] A. L. Cavalieri, N. Müller, T. Uphues, V. S. Yakovlev, A. Baltuška, B. Horvath, B. Schmidt, L. Blümel, R. Holzwarth, S. Hendel, M. Drescher, U. Kleineberg, P. M. Echenique, R. Kienberger, F. Krausz, and U. Heinzmann, Attosecond spectroscopy in condensed matter, *Nature (London)* **449**, 1029 (2007).
- [14] M. Sabbar, S. Heuser, R. Boge, M. Lucchini, T. Carette, E. Lindroth, L. Gallmann, C. Cirelli, and U. Keller, Resonance effects in photoemission time delays, *Phys. Rev. Lett.* **115**, 133001 (2015).
- [15] J. Mauritsson, M. B. Gaarde, and K. J. Schafer, Accessing properties of electron wave packets generated by attosecond pulse trains through time-dependent calculations, *Phys. Rev. A* **72**, 013401 (2005).
- [16] M. Swoboda, T. Fordell, K. Klünder, J. M. Dahlström, M. Miranda, C. Buth, K. J. Schafer, J. Mauritsson, A. L'Huillier, and M. Gisselbrecht, Phase measurement of resonant two-photon ionization in Helium, *Phys. Rev. Lett.* **104**, 103003 (2010).
- [17] D. Guénot, D. Kroon, E. Balogh, E. W. Larsen, M. Kotur, M. Miranda, T. Fordell, P. Johnsson, J. Mauritsson, M. Gisselbrecht, K. Varjù, C. L. Arnold, T. Carette, A. S. Kheifets, E. Lindroth, A. L'Huillier, and J. M. Dahlström, Measurements of relative photoemission time delays in noble gas atoms, *J. Phys. B: At. Mol. Opt. Phys.* **47**, 245602 (2014).
- [18] C. Palatchi, J. M. Dahlström, A. S. Kheifets, I. A. Ivanov, D. M. Canaday, P. Agostini, and L. F. Dimauro, Atomic delay in helium, neon, argon and krypton, *J. Phys. B: At. Mol. Opt. Phys.* **47**, 245003 (2014).
- [19] E. S. Toma and H. G. Muller, Calculation of matrix elements for mixed extreme-ultraviolet–infrared two-photon above-threshold ionization of argon, *J. Phys. B: At. Mol. Opt. Phys.* **35**, 3435 (2002).

- [20] R. Pazourek, S. Nagele, and J. Burgdörfer, Attosecond chronoscopy of photoemission, *Rev. Mod. Phys.* **87**, 765 (2015).
- [21] R. Pazourek, S. Nagele, and J. Burgdörfer, Time-resolved photoemission on the attosecond scale: Opportunities and challenges, *Faraday Discuss.* **163**, 353 (2013).
- [22] M. Ivanov and O. Smirnova, How accurate is the attosecond streak camera? *Phys. Rev. Lett.* **107**, 213605 (2011).
- [23] G. Schmid, K. Schnorr, S. Augustin, S. Meister, H. Lindenblatt, F. Trost, Y. Liu, N. Stojanovic, A. Al-Shemmary, T. Golz, R. Treusch, M. Gensch, M. Kübel, L. Foucar, A. Rudenko, J. Ullrich, C. D. Schröter, T. Pfeifer, and R. Moshhammer, Terahertz-field-induced time shifts in atomic photoemission, *Phys. Rev. Lett.* **122**, 073001 (2019).
- [24] U. Saalmann and J. M. Rost, Proper time delays measured by optical streaking, *Phys. Rev. Lett.* **125**, 113202 (2020).
- [25] H. D. Cohen and U. Fano, Interference in the photo-ionization of molecules, *Phys. Rev.* **150**, 30 (1966).
- [26] J. Fernández, O. Fojón, A. Palacios, and F. Martín, Interferences from fast electron emission in molecular photoionization, *Phys. Rev. Lett.* **98**, 043005 (2007).
- [27] S. E. Canton, E. Plésiat, J. D. Bozek, B. S. Rude, P. Declava, and F. Martín, Direct observation of Young's double-slit interferences in vibrationally resolved photoionization of diatomic molecules, *Proc. Natl. Acad. Sci. USA* **108**, 7302 (2011).
- [28] D. Akoury, K. Kreidi, T. Jahnke, Th. Weber, A. Staudte, M. Schöffler, N. Neumann, J. Titze, L. Ph. H. Schmidt, A. Czasch, O. Jagutzki, R. A. Costa Fraga, R. E. Grisenti, R. Díez Muiño, N. A. Cherepkov, S. K. Semenov, P. Ranitovic, C. L. Cocke, T. Osipov, H. Adaniya, J. C. Thompson, M. H. Prior, A. Belkacem *et al.*, The simplest double slit: interference and entanglement in double photoionization of H_2 , *Science* **318**, 949 (2007).
- [29] S. X. Hu, L. A. Collins and B. I. Schneider, Attosecond photoelectron microscopy of H_2^+ , *Phys. Rev. A* **80**, 023426 (2009).
- [30] X. X. Guan, E. B. Secor, K. Bartschat, and B. I. Schneider, Double-slit interference effect in electron emission from H_2^+ exposed to x-ray radiation, *Phys. Rev. A* **85**, 043419 (2012).
- [31] Y. Li, M. Qin, X. Zhu, Q. Zhang, P. Lan, and P. Lu, Ultrafast molecular orbital imaging based on attosecond photoelectron diffraction, *Opt. Express* **23**, 10687 (2015).
- [32] X. Y. Lai, S. P. Xu, S. G. Yu, M. W. Shi, W. Quan, and X. J. Liu, Revealing the wave-function-dependent zeptosecond birth time delay in molecular photoionization with double-slit interference minima, *Phys. Rev. A* **104**, 043105 (2021).
- [33] K. Liu, Y. Hu, Q. Zhang, and P. Lu, Nondipole effects on the double-slit interference in molecular ionization by xuv pulses, *Opt. Express* **29**, 38758 (2021).
- [34] C. J. Joachain, N. J. Kylstra, and R. M. Potvliege, Atoms in intense, ultrashort laser pulses: Non-dipole and relativistic effects, *J. Mod. Opt.* **50**, 313 (2003).
- [35] B. Feuerstein and U. Thumm, Fragmentation of H_2^+ in strong 800-nm laser pulses: Initial-vibrational-state dependence, *Phys. Rev. A* **67**, 043405 (2003).
- [36] K. Liu, W. Hong, and P. Lu, Phase dependence of electron localization in HeH^{2+} dissociation with an intense few-cycle laser pulse, *Opt. Express* **19**, 20279 (2011).
- [37] Y. Hu, K. Liu, Q. Ma, and P. Lu, Multielectron effect in XUV light-driven strong-field ionization beyond the dipole approximation, *J. Opt. Soc. Am. B* **39**, 2486 (2022).
- [38] K. Liu and I. Barth, Identifying the tunneling site in strong-field ionization of H_2^+ , *Phys. Rev. Lett.* **119**, 243204 (2017).
- [39] Y. Fu, J. Zeng, and J. Yuan, PCTDSE: A parallel Cartesian-grid-based TDSE solver for modeling laser-atom interactions, *Comput. Phys. Commun.* **210**, 181 (2017).
- [40] Z.-H. Zhang and F. He, Photoionization of H_2^+ beyond the dipole approximation with zeptosecond time resolution, *Phys. Rev. A* **103**, 033112 (2021).
- [41] H. Liang, S. Grundmann, Y. K. Fang, L. Geng, Q. Gong, and L. Y. Peng, Nondipole effects in interference patterns of a two-electron wave, *Phys. Rev. A* **104**, L021101 (2021).
- [42] I. A. Ivanov, A. S. Kheifets, and K. T. Kim, Effect of the finite speed of light in ionization of extended molecular systems, *Sci. Rep.* **11**, 21457 (2021).